

Ground-state energy of quasi-free positrons in non-polar fluids

Eve Cheng,¹ Daniel Cocks,¹ and Robert P. McEachran¹

Research School of Physics, Australian National University, Canberra

(Dated: November 3, 2021)

We have calculated the background energy (V_0) for positrons in noble gases with an *ab initio* potential and the Wigner-Seitz (WS) ansatz. In contrast to the general pseudo-potential approach, we have used accurate *ab initio* potentials for the positron-atom interaction. The ansatz includes an assumed form of the potential, resulting from an average over fluid atoms, and we propose four different options for this. By comparing the different options to literature data for effective electron number (Z_{eff}), we find that agreement can be obtained for light elements, but fails for heavy elements. We suspect that the strong polarizability of the heavy elements makes the simple potential averaging, as assumed in the Wigner-Seitz model, insufficient to fit the measurements without also making use of pseudo-potentials. We also raise our suspicion that the comparison of annihilation rates between ground-state calculations and experimental values is not appropriate. Furthermore, the congruence of V_0 to Z_{eff} values predicted by a contact potential approximation appears to be invalidated by our results.

Many technological applications involve the movements of electrons/positrons through a fluid, including medicine, industry and some environmental advances¹⁻³. Hence, it is vital to understand the mechanisms behind the transport of quasi-free electrons/positrons, and how they can be accurately simulated⁴. While the positron/electron propagation has been extensively studied theoretically in dilute gases⁵⁻⁹, the theoretical basis for positron propagation in liquids is unsatisfactory. As most experimental comparisons have been made with electrons, positrons offer a unique opportunity to test the core assumptions and improve the predictive power of theoretical models. Therefore in this paper, we focus on the effects of density on the propagation of positrons in fluids.

The density dependence of the propagation of positrons in liquids is more challenging than in dilute gases. Because of the closer proximity in liquids, clusters or bubbles among other phenomena can occur because of the density-dependence of the charged particle/fluid interaction^{5,10-13}. This paper will focus on the propagation of the positron in homogeneous media, as understanding this intrinsic behaviour is necessary to understand those more complicated phenomena.

One noticeable density dependent property of a fluid is the non-negligible background contribution it makes to propagating states, often referred to as "quasi-free" states. The background contribution is evident in the lowest energy that a quasi-free particle can have, known as V_0 ⁵, sometimes referred to as the self energy¹⁴. The values for V_0 can be on the order of a fraction of an eV below, or above, the vacuum energy. Because V_0 affects the resulting wavefunction of the particle, it is required for calculating its effective scattering behaviours, such as the annihilation rate for positrons. It also influences the

ionisation potential of any atoms/molecules in fluids. In addition, V_0 provides the barrier at liquid-gas interfaces, which can lead to some interesting properties^{15,16}. Therefore, in this paper, we focus on the density dependence of V_0 for positrons in fluids of the noble-gas atoms ranging from gas to liquid densities.

For low density fluids, the linear density dependence of V_0 can be estimated by the optical pseudo-potential approximation⁵. We will later show that this may be a bad approximation even in the limit of zero-density, where many-body effects could be expected to be negligible. In dense fluids, it is clear that the potential can no longer be simplified by a contact potential; the density dependence of V_0 is no longer linear.

There have been many experimental attempts to obtain V_0 for electrons in non-polar fluids¹⁵⁻¹⁷. The most intuitive experimental approach is to measure the photoemission thresholds of a metal surface in vacuum and the target fluid^{17,18}. However, this approach is limited because of the possible contamination and coating of the metal surface. Instead, Evans and co-workers¹⁶ proposed a different indirect approach that obtains V_0 by measuring the photoionization spectrum for the metal surface in liquids under two electric fields. They have measured V_0 for electrons in liquid Ar, Kr, He, Ne, N₂, CO₂, methane and ethane¹⁹⁻²⁵. Borghesani¹⁵ measured V_0 for electrons using the resonance attachment frequency of electrons to oxygen molecules. The V_0 values were calculated by comparing the attachment frequencies of the electrons in vacuum and target liquid.

All experimental approaches for V_0 in fluids so far are limited to electrons only. There is no experimental data on V_0 values for positrons due to the difficulty of creating quasi-free positrons at low energies inside of a fluid. There

was one study done on the V_0 calculations and measurements in solids²⁶, which was used to compare to the V_0 calculation in liquids in the study. Fortunately, there are some indirect approaches, which obtain V_0 by measuring the effective number of electrons the positron can annihilate with per atom in a fluid, commonly referred to as Z_{eff} ²⁷.

There have been several existing theoretical approaches to calculate V_0 in fluids. The "finite size" approach^{28,29} finds a solution locally within a finite system and then extrapolates to the macroscopic scale. The Schrödinger equation was solved by mapping the electron wavefunction to an isomorphic polymer chain using Monte Carlo methods²⁸. There are also other similar approaches that evaluate the electron wavefunction on a small grid and then extrapolate to larger systems²⁹. These approaches are computationally limited, as only small systems can be simulated in this way, although advances in numerical techniques have pushed this to an impressive scale³⁰.

The "focus atom" approach was first used by Springett and coworkers³¹. The approach uses the Wigner-Seitz (WS) model, which models the fluid as a collection of spherical unit cells centered around each liquid atom. In order to find V_0 by solving the Schrödinger equation, they calculate the potential interaction between the electrons and the fluid by focusing on the interaction between the electron and a focus atom, and then calculating the total effective interaction as the ensemble average. Since then a wide range of studies of the noble-gases and non-polar molecules have been performed, see Holroyd and Schmidt³² and Iakubov and Khrapak⁵ and references therein for reviews of the original forays into this field. Many improvements on the pseudo-potentials used in the theory were made, along with techniques to include features of the interaction that could not be addressed by the pseudo-potentials^{11,33-35}. Recently, another advancement on this calculation method was published by Evans and co-workers¹⁶ later along with their experimental results. This study is built upon the original WS model through introducing the concept of local WS cell (LWS) radius; it calculates V_0 for electrons as a combination of the ensemble polarization energy, the kinetic energy and the thermal energy. A series of calculations and experiments were performed^{16,36} through a wide variety of species, including the noble gas atoms and simple hydrocarbons. The results showed significant agreement between the model and experimental data for electrons.

While the "focus atom" approaches focus on finding reasonable approximations to the potential in the vicinity of one atom and taking an average of the rest of the atoms in the fluid, alternative techniques were also proposed. Some studies^{37,38} focus on the representation of the transition

matrix, considering averages over multi-particle terms³⁸ or diagrammatic approaches with vertex terms³⁷.

This paper calculates V_0 using the "focus atom" method and solves the Schrödinger equation for the positron directly with both WS and LWS radius. The purpose of using both options for the radius is to test the extensibility of the LWS method by applying it to positrons, using accurate positron-atom potentials without free parameters. However, we also extend upon the previous approaches to include four different options for including the contribution to the potential felt by the positron from the atoms surrounding the focus atom. We contrast these approaches and their suitability.

The structure of this paper is as follows: the first section is dedicated to the theory for our calculations. It goes through the Schrödinger equation that we solve, the potential term in the equation and the corresponding boundary conditions used. The screening function and the calculation for Z_{eff} are also discussed. The second section describes the numerical implementation using an in-house program PEEL (calculator of Positron and Electron Energy in Liquids). The third section goes through the results generated from the program and discusses the implications and potential future work and publications.

I. THEORY

The value of V_0 describes the lowest energy that a positron can have in a particular fluid. In this paper, we find V_0 by solving for an approximate solution to the Schrödinger equation for the wavefunction of the positron in fluids with an ansatz. Our method is related to that of Springett *et al*³¹, and Evans *et al*¹⁶, although the derivation itself differs.

In our approach, we first decouple the motion of the positron from the atoms by freezing the atomic positions, which is similar to Springett *et al*³¹. Consequently, we aim to solve the single-particle Schrödinger equation for the many-body system.

We solve this equation by taking an ansatz for the wavefunction. Same with the WS model, we define the liquid as a collection of WS cells. We then separate the liquid environment into two regions: inside or outside of the WS cells. Inside the WS cells, the potential and the corresponding ground-state wavefunction are spherically symmetric; outside the cells, the potential is V_0 , and the corresponding wavefunction is constant:

$$\psi_{k_i}(\mathbf{r}) = \begin{cases} R(\mathbf{r}) & r < r_{\text{cell}} \\ \text{const} & r > r_{\text{cell}} \end{cases} \quad (1)$$

The necessary boundary condition to connect the inside/outside regions is that the first derivative of the wavefunction at the edge of the WS cells is zero:

$$(\partial\psi_0/\partial r)|_{r=r_{\text{cell}}} = 0 \quad (2)$$

where the quantity r_{cell} , the radius of the cell, can take two different values in this paper. The conventional choice is $r_{\text{cell}} = r_{WS}$, where the Wigner-Seitz radius is given as

$$r_{WS} = \left(\frac{3}{4\pi\rho_0}\right)^{1/3}. \quad (3)$$

where ρ_0 is the atomic density of the fluids.

This effectively partitions the entire fluid volume into equal volumes for each atom. Based on the ansatz for the wavefunction, it is clear that the WS model assumes no overlap among WS cells. However, because the atoms in fluids fluctuate, this restriction of no overlap cannot be guaranteed physically. Therefore, it is our intention to acknowledge this limitation of the WS model and deal with the potential overlaps among WS cells; this is reflected in our definitions of the potential interaction later.

Another definition for the cell radius was proposed by Evans *et al*¹⁶. Instead of partitioning the WS cells equally, the radius was adjusted to a smaller value, $r_{\text{cell}} = r_{LWS}$, which takes account of the pair correlator in the liquid. The new radius is called the local WS (LWS) cell radius:

$$r_{LWS} = \left(\frac{3}{4\pi\rho_0 g_{max}}\right)^{1/3} \quad (4)$$

where g_{max} represents the maximum of the pair correlation function, $g(r)$ (discussed in further detail below).

For electrons, the LWS radius is shown to lead to reasonable agreement between theory and experiments in dense fluid systems¹⁶, and does very well at predicting the behaviour around the critical point. We investigate both WS and LWS radius to observe the effects of different radii on the resulting V_0 values; this should also tell us whether the LWS radius can be extended to positrons or not.

Since the boundary condition requires the corresponding wavefunction to be spherically symmetric in each cell, we find V_0 by solving the single-particle Schrödinger equation within a cell:

$$\left[\frac{d^2}{dr^2} - U(r) + k^2\right]u(r) = 0 \quad (5)$$

where $\frac{\hbar^2}{2m}U(r)$ is the total positron-atom interaction, k is the wavenumber and $u(r)/r$ is the total radial wavefunction.

We note here that while the WS model is sufficient in calculating the ground-state eigenvalue, it does not provide the infrastructure to calculate higher energy states with non-zero momentum. The boundary condition of WS model forces the wavefunction to be spherically symmetric, which does not accommodate higher energy states. Our future goal is to calculate the bandstructure of the liquid; it would require a completely new approach, and it will be discussed in future work.

A. The total potential in fluids

The difference between our approach and the traditional WS approach³¹ lies in our potential term. Our total potential for the interaction between the positron and all atoms is treated as precisely as possible for one atom (referred to as the "focus atom"), and averaged for all others. In terms of the interaction between the focus atom and the positron, instead of using pseudopotentials as most of the WS approaches^{16,26,31}, we use an *ab initio* potential, which has been verified against single scattering cross sections^{39,40}. There are also modifications implemented to the averaging of the potential, which will be elaborated in this section.

In short, our total potential can be written as:

$$U = U_1 + U_2 \quad (6)$$

where U is the total potential, U_1 is the contribution of the focus atom, including screening effects, and U_2 is the contribution from the surrounding atoms.

We define the focus atom as an atom within a neighbourhood of the WS radius of the positron; this neighbourhood changes as the positron moves through the fluid. Because we acknowledge the overlap among WS cells, there might not be a unique choice for the focus atom; this ambiguity will be addressed later when defining U_2 .

1. Focus atom interaction with the positron U_1

The interaction between a positron and an isolated atom (V) can be described using the polarized orbital method⁴⁰, which separates the potential into two parts: the static (U_s) and the polarization potential (U_p). The static potential represents the Coulomb interactions with the unperturbed Dirac-Fock orbitals, whereas the polarization potential is given by a multipole expansion up to octopole terms in the perturbation of the orbitals. Due to the lack of exchange interaction, the representation of

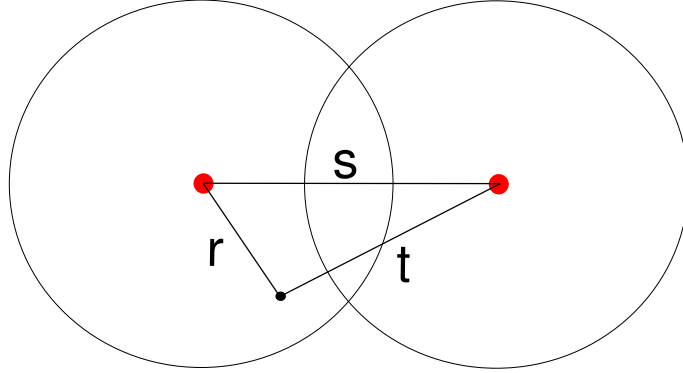


Figure 1: This diagram depicts our method for calculating the average potential interaction between the positron and the liquid atoms. The red dots represent the atoms, while the black small dot represents the positron. The left red dot is the focus atom, while the right red dot is a randomly selected neighbouring atom. The variables r , s , t are consistent with equation (8) and the definitions for the interaction potentials.)

the polarisation interaction in positron scattering is more important than in electron scattering.

In a liquid, the interaction between the positron and the focus atom (U_1) can only be partially described by (V) above. In addition to V , we must account for screening⁴¹. The basic element of screening involves the cooperation between each pair of atoms, as depicted in Figure 1. The variables r , s , and t refer to the positron-focus atom, atom-atom, and positron-neighbouring atom distances respectively. With all considered, U_1 can be expressed as:

$$U_1 = U_s + f(r)U_p, \quad (7)$$

where $f(r)$ is a screening function.

Assuming that the largest contribution to screening comes from the dipole-dipole interaction between the atoms, we may use the well-known⁴¹ self-consistent expression for $f(r)$:

$$f(r) = 1 - \pi n \int_0^\infty ds s^{-2} g(s) \int_{|r-s|}^{r+s} dt t^{-2} f(t) \alpha(t) \Theta(r, s, t) \quad (8)$$

where $g(s)$ is the radial distribution function, and $\alpha(r)$ is the dipole polarisability as a function of r , which is the dominant contribution to U_p and,

$$\Theta = \frac{3}{2} s^{-2} (s^2 + t^2 - r^2)(s^2 + r^2 - t^2) + (r^2 + t^2 - s^2). \quad (9)$$

We obtain $f(r)$ by iterating (8), starting from a constant value $f(r) = f_L$ where f_L is the Lorentz local field:

$$f_L = 1/(1 + (8/3)\pi n \alpha), \quad (10)$$

and $\alpha = \alpha(r \rightarrow \infty)$ is the asymptotic dipole polarisability.

While the most obvious effect that the surrounding atoms have on the focus-atom-positron interaction is the polarization reduction from static screening, there are other effects that we have neglected. For example, dynamic polarization is difficult to handle even for the case of single-atom positron scattering, so we do not include the effects of surrounding atoms on the focus-atom dynamic polarizability.

2. The effective potential between the surrounding atoms and the positron U_2

As mentioned above, the acknowledgment of the overlap among WS cells has certain implications when defining U_2 . Because of the existence of overlaps, there can be more than one atom within the neighbourhood of WS radius centering the positron. If no other limitations are applied, the interaction between a positron and the liquid environment (denoted as U_2^T) can be calculated as an ensemble average of the single atom interaction potential:

$$U_2^T(r) = \frac{2\pi\rho}{r} \int_0^\infty dt t U_1(t) \int_{|r-t|}^{r+t} ds s g(s), \quad (11)$$

The U_2^T option for U_2 assumes no correlation between the positron and the surrounding atoms and relies solely on the atom-atom correlation $g(r)$. This is the simplest choice because it averages over the positron-surrounding atom separation. It effectively assumes a Born-approximation-like interaction between the positron and surrounding atom. Hence, it includes large unphysical contributions from the divergent static potential.

While still enforcing no additional constraints on the identity of the focus atom, the second option (U_2^P) for U_2 takes only the ensemble average of the polarization potential U_p to avoid the divergent spike of the static potential as $t \rightarrow 0$:

$$U_2^P(r) = \frac{2\pi\rho}{r} \int_0^\infty dt tU_p(t) \int_{|r-t|}^{r+t} ds sg(s) \quad (12)$$

The U_2^P option assumes the atoms are far away from each other enough that the static potential coming from non-focus atoms does not contribute to the interaction, although it does allow short-range contributions from the polarisation potential. This tends to over-emphasise the potential interactions and therefore serves as a lower bound to V_0 .

Our third and fourth options (U_2^r and $U_2^{U_1}$) apply a cut-off radius, r_0 when calculating U_2 . The general form of U_2 for these two options is:

$$U_2^R(r; r_0) = \frac{2\pi\rho}{r} \int_{r_0}^\infty dt tU_1(t) \int_{|r-t|}^{r+t} ds sg(s) \quad (13)$$

The application of a cut-off radius applies additional constraint on the identity of the focus atom. The only difference between equation (11) and (13) is that equation (13) integrates from r_0 instead of 0 in the outer integral (i.e. $U_2^T(r) = U_2^R(r; 0)$). This seemingly minor difference marks the focus atom to be the closest atom to the positron, acting as a second barrier upon $g(r)$ to keep atoms at reasonable distances from the positron. This is a reasonable choice for dense fluids, where the close packing forces this behaviour.

The third option (U_2^r) takes the choice of $r_0 = r$:

$$U_2^r(r) = U_2^R(r; r). \quad (14)$$

In comparison, the fourth method ($U_2^{U_1}$) sets $r_0 = r_{U_1}$, where r_{U_1} is the radius where U_1 first crosses the r axis, i.e. $U_1 = 0$:

$$U_2^{U_1}(r) = U_2^R(r; r_{U_1}). \quad (15)$$

This method assumes the positron is kept away from the core of the surrounding atoms by the repulsive static part of the potential. This method captures the main effects of U_2^P with some additional repulsive interactions included.

The implementation of the LWS radius method for the potential is the same as the WS radius method, except V_{WS} is defined as the spherical space with radius of the local WS radius instead.

A cut-off radius was often implemented in many existing WS approaches^{16,26,31} in a very different manner than

ours. In the existing approaches, they use the sum of the hard-sphere static potential and the polarisation potential with a pre-defined cutoff radius to calculate U_1 ^{16,26,31}. Different from those approaches which apply cut-off radii to the total potential, we use the full U_1 and only apply cut-off radii to U_2 . We believe cut-offs in this fashion can potentially lead to more accurate results.

B. The effective charge Z_{eff}

Because there is no experimental data for V_0 values in the liquid phase, instead, we can draw a comparison between the effective charge, Z_{eff} , of our calculated ground state, and measured annihilation rates. The effective charge is calculated through determining the wavefunction overlap between the charged particle and the electron cloud around the focus atom in the liquid²⁷.

$$Z_{\text{eff}} = \sum_{i=1}^N \int |\Psi(\mathbf{r}_1, \mathbf{r}_2, \dots, \mathbf{r}_N; \mathbf{x})|^2 \delta(\mathbf{r}_i - \mathbf{x}) d\mathbf{r}_1 d\mathbf{r}_2 \dots d\mathbf{r}_N \quad (16)$$

where Ψ is the total wavefunction of electron with \mathbf{x} being the position vector of the positron, and \mathbf{r}_i refers to the coordinates of the atomic electrons (spin included).

The Z_{eff} can also be written as^{8,27}:

$$Z_{\text{eff}} = Z_{\text{eff}}^0 + Z_{\text{eff}}^1 \quad (17)$$

where

$$Z_{\text{eff}}^i = \int_0^\infty d\mathbf{r} |\psi(\mathbf{r})|^2 \rho_i(\mathbf{r}) \quad (18)$$

where $\rho_0(\mathbf{r})$ represents the unperturbed charge density of the atomic orbitals, and $\rho_1(\mathbf{r})$ refers to the first-order correction due to the polarization interaction between the electrons and the positron. It can be easily shown that equation (17) is equivalent to equation (16).

We also extend the definition of the Z_{eff} to include the electron density contribution from the surrounding atoms²⁷:

$$Z_{\text{eff}} = \frac{1}{n} \int_0^{r_m} d\mathbf{r} (\rho_L(\mathbf{r}) + \rho_S(\mathbf{r})) |\Psi(\mathbf{r})|^2 \quad (19)$$

$$= Z_{\text{eff}}^L + Z_{\text{eff}}^S \quad (20)$$

Note that Z_{eff}^L here is equivalent to the Z_{eff} in equation (17). Our calculation shows the contribution from Z_{eff}^S is negligible for all gases.

C. The averaged effective charge $\langle Z_{\text{eff}} \rangle$

All of our calculations so far assume k (the wavenumber) $\rightarrow 0$, however, this is not realistic for experimental measurements. In order to make some better comparisons with experiment, we also performed preliminary calculations of the thermally averaged Z_{eff} , i.e. $\langle Z_{\text{eff}} \rangle$.

We assume the thermal distribution for the positron is a Boltzmann distribution, and therefore the thermal average for Z_{eff} can be represented by:

$$\langle Z_{\text{eff}} \rangle = \int_0^\infty dE W_b(E) \times Z_{\text{eff}}(E) \quad (21)$$

$$W_b(E) = N \times \sqrt{E} \exp\{-E/kT\} \quad (22)$$

$$N = \int_0^\infty dE \sqrt{E} \exp\{-E/kT\} \quad (23)$$

where $W_b(E)$ is the Boltzmann weight factor for each thermal energy, $Z_{\text{eff}}(E)$ is the Z_{eff} value for the thermal energy E , and N is the normalization factor for the Boltzmann weight factor. In our numerical implementation, we truncate the integration over E at an upper limit of $15kT/2$ rather than infinity.

II. NUMERICAL IMPLEMENTATION (PEEL)

We have developed an in-house program called PEEL: calculator of Positrons and Electrons Energy in Liquids.

A. Inputs for the Potential Calculation

For atomic species, a tabulated set of values for U_p and U_s has been calculated, using the Dirac-Fock orbitals of the atom, as described in⁸ but with updated parameters. We have calculated the screening function, $f(r)$, iteratively from equation (8) using the radial distribution functions, and the dipole polarisability $\alpha(r)$ of the potential calculation.

1. The radial distribution function $g(r)$

The radial distribution function $g(r)$ is calculated iteratively solving the Ornstein-Zernike relation with Percus-Yevick approximation⁴²:

$$\exp[\beta v(r)]g(r) = 1 + \rho \int [g(r-r') - 1]g(r') \quad (24)$$

$$(1 - \exp[\beta v(r')])dr'$$

where $v(r)$ is the pair potential between the liquid atoms and β represents the thermal energy.

We simplified the pair potential between two liquid atoms to be the Lennard-Jones potential for the $v(r)$ calculation:

$$U(r) = 4\epsilon \left[\left(\frac{\sigma}{r}\right)^{12} - \left(\frac{\sigma}{r}\right)^6 \right] \quad (25)$$

where $U(r)$ represents the interatomic potential energy, ϵ is the depth of the potential well (the liquid atoms), and σ is the distance at which the interatomic potential interaction becomes zero. The values for ϵ and σ were generated through fitting for viscosity data of different fluids⁴³. This is a commonly used model potential, which approximates the hard-core repulsion and van-der-Waals interaction of real atomic interactions.

An empirically deduced form of the reduced temperature was used in solving the Ornstein-Zernike relation⁴³.

$$T^* = \frac{k_B(T - \tau)}{\epsilon} \quad (26)$$

where k_B is thermal energy, and τ is the correction factor that is also generated through fitting the viscosity data.

We have also checked the results using a molecular dynamic package Large-scale Atomic/Molecular Massively Parallel Simulator (LAMMPS) at selected densities and temperatures⁴⁴. The iterative function is preferred because it is significantly less computationally expensive compared to LAMMPS.

B. Scattering equation solver

With the potential implemented, the program solves the Schrödinger equation for the ansatz given in equation (2) with the lowest energy eigenvalue that satisfies the boundary condition.

With the potential term implemented using equation (6), PEEL was set up to solve for the wavefunction with a given energy from $r = 0$ to $r = r_m$ (where r_m is the cell radius). This uses the Julia package DifferentialEquations with callbacks to handle divergent behaviour in the classically forbidden region. Once the wavefunction is calculated, the program will provide both the values of the wavefunction and the derivative of the wavefunction.

The most intuitive way to ensure the boundary condition for equation (5) would be to run the wavefunction solver for a range of energies and record the one that satisfies the WS boundary condition with the expected number of turning points. The turning points refer to the points on the wavefunction where its derivative is zero,

and V_0 corresponds to the wavefunction with only one turning point. This method can be used but tends to be very slow and relies heavily on the grid of input energies.

However, to speed up the process and improve the accuracy of calculating V_0 , a root-finding method was implemented instead of the intuitive one. The root-finding method searches for the root of a turning-point-counting function, which counts the number of turning points in a wavefunction within a range of energies. In order to increase the accuracy and speed, the range of energies is narrowed down first. The upper-limit is set as the lowest energy eigenstate for bound-state wavefunction. The lower-limit was calculated by finding out an energy corresponding to the wavefunction with no turning points. Once the energy range is calculated, we search for the root of the turning-point-counting function within the energy range calculated. The resulting root is V_0 .

III. RESULTS

The result section is structured as follows: we first focus on the four options for the form of U_2 and use argon as a test case to explore the density dependence of both V_0 and Z_{eff} for each option. We also discuss the effects of the inclusion of the Boltzmann thermal distribution of the incoming positron to the calculation for argon. We then select one of these methods to explore the other noble gases: helium, neon, krypton and xenon.

A. Density dependence of V_0 for argon

Our results for the V_0 values of positrons in fluid argon using the different averaging options are shown in figure 2a) for the choice of $r_{\text{cell}} = r_{\text{WS}}$. A similar comparison is made in figure 2b) but for $r_{\text{cell}} = r_{\text{LWS}}$.

In general, the qualitative behaviour is very similar for the different options of averaging, i.e. the contribution to the potential from U_2 . All V_0 values are negative, which is consistent with the scattering length of positron scattering from argon (see table I). As the density increases, V_0 steadily increases in magnitude, which means the interaction between the positron and the fluid becomes more attractive with higher densities; this is also expected.

In the limit of low densities, a linear dependence on density for $V_0(\rho \rightarrow 0)$ is observed in our results (see Figure 2). This linearity is consistent with Iakubov and Khrapak's derivation⁵, which uses a contact potential approximation for the positron-atom interaction:

$$V(r) \approx \frac{2\pi\hbar^2}{m} a_s \delta(r) \quad (27)$$

Under the contact potential approximation, V_0 depends linearly on the density and the scattering length, a_s :

$$V_0 \approx \frac{2\pi\hbar^2}{m} a_s \rho \quad (28)$$

Since the scattering lengths are usually readily available, the slope of $V_0(\rho \rightarrow 0)$ is commonly used as a benchmark for low density regions (see Table I).

Compared to the contact potential approximation, our potential ($U(r)$) for the positron-atom interaction is calculated in a more precise manner. While U_1 should be consistent with the scattering length, one can view the four options provided for U_2 as alternatives to the contact potential approximation. In this way, we can characterise the combined effects of the dilute fluid on the positron via a single quantity: $\lim_{\rho \rightarrow 0} dV_0/d\rho$. One can draw an analogy between this quantity and the scattering length, which characterises single-atom scattering for low energy, as both are directly relevant to experiments in a particular limit and both result from the full set of interactions in the system. Similarly, the contact potential is the "idealized case" for both of these quantities, and in a fluid this can be seen in the linear dependence in equation (28). It should be pointed out, however, that our use of a ranged potential means $dV_0/d\rho$ will quickly deviate from its value in the dilute limit as denser fluids are considered.

At low densities, the inclusion of U_2 causes the linear trend of $V_0(\rho \rightarrow 0)$ to deviate from the contact potential approximation; it preserves the linearity of $V_0(\rho \rightarrow 0)$ but changes its gradient. The two choices U_2^T and U_2^P under- and over-estimate this low-density trend, and therefore serve as clear upper/lower bounds for $V_0(\rho \rightarrow 0)$. As the upper bound, U_2^T weights the entire repulsive static potential equally, even for $r \rightarrow 0$ where the positron wavefunction is suppressed, and consequently underestimates the slope. As the lower bound, U_2^P completely neglects the static potential and therefore overestimates the slope. Inbetween two bounds, the option U_2^R potentially underestimates the contribution from the polarisation potential interaction and consequently could result in overestimation of the slope. The option U_2^{U1} produces V_0 values between U_2^P and U_2^T at low densities.

As the density increases in the low density region, the positron becomes more confined in the fluid, which in turn leads to a strong kinetic energy contribution. Because of the increasing contribution from the repulsive interaction between the positron and the nuclei at higher densities,

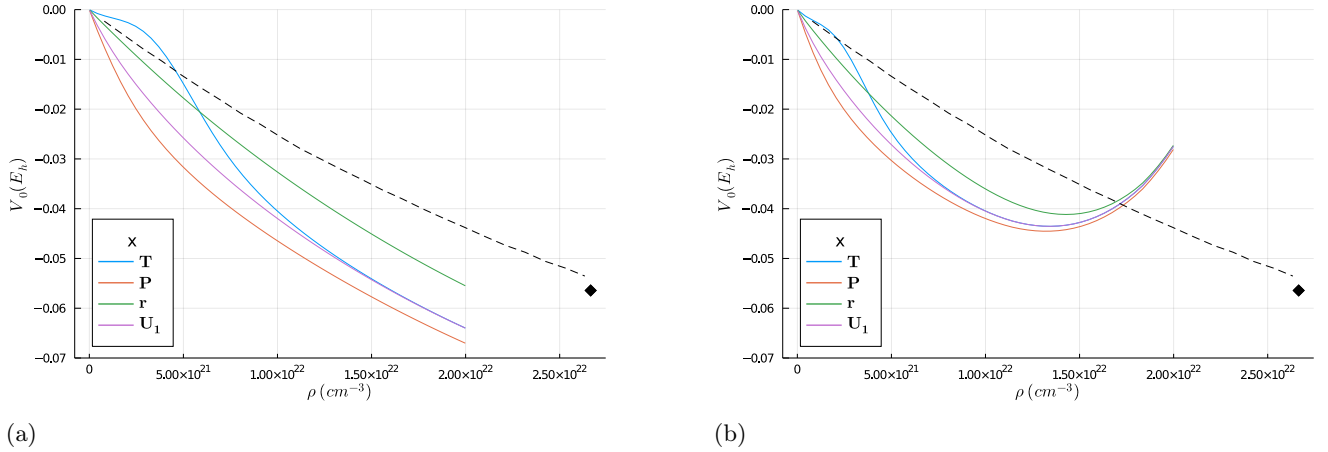


Figure 2: The density dependence of V_0 for argon at 295K. (a) V_0 calculation with $r_{\text{cell}} = r_{\text{WS}}$ (b) V_0 calculation with $r_{\text{cell}} = r_{\text{LWS}}$. The lines correspond to the different options for U_2^x , where x is shown in the legend. The black dashed lines in (a) and (b) come from the theoretical studies²⁶ using a simple pseudo-potential comprised of hard-sphere core and dipole polarization terms. The black diamonds in (a) and (b) refer to the experimental results obtained in crystalline samples at 4 K⁴⁵.

the resulting V_0 values are expected to decrease with a slower rate. This expectation is met with all methods except U_2^T , because it over-estimates the repulsive interaction at lower densities.

We expect that at sufficiently high densities, the repulsive interaction dominates the positron-fluid interaction and leads to an increasing trend in V_0 . This appears in the case of $r_{\text{cell}} = r_{\text{WS}}$ as a flattening of the slope, and is much more dramatic for the $r_{\text{cell}} = r_{\text{LWS}}$ case due to the smaller effective sphere allowed for the positron. In fact, r_{LWS} provides a turning point in $V_0(\rho)$. The existence of a turning point allows the potential to describe fluctuation clustering in fluids, where a positron can cause the a local fluctuation in density towards the point of $dV_0/d\rho = 0$. This can be seen, for example, with clustering in helium caused by positrons; it is observed that clusters of fixed density form independently of the background fluid density⁴⁶.

While there is a difference in the density dependence of V_0 at high densities with respect to the choice of r_{cell} , the relative position of V_0 curves using four different methods is roughly the same. The U_2^P method still acts as the lower bound for V_0 calculations. Interestingly, U_2^T , instead of U_2^P , serves as the upper bound at high densities, for both r_{cell} choices. This switch is due to the different sources for the overestimation of V_0 for these two methods. U_2^T overestimates V_0 through overestimation of repulsive interaction, while U_2^P underestimates the polarisation interaction. In addition, we have observed

that the calculations from $U_2^{U_1}$ tend to converge to U_2^T at high densities; we think this is because r_{cell} is small enough at high densities that the positron is not allowed to be too close to other atoms even with option U_2^T .

Among the four averaging choices, the U_2^T choice shows an unusual feature by having initially a smaller slope at low densities. As previously discussed, this is likely due to its indiscriminate inclusion of the entire static potential and suggests that it is a poor choice for low densities. Note that we have used this choice in the past for cross section calculations of electron scattering in fluids^{27,39} as it is the simplest description of the surrounding average.

The results from previous theoretical calculations by Pleniewicz *et al*²⁶ are shown in Figure 2 as comparison for our calculations. Overall, their V_0 results are consistently higher than our results. At low densities, the slopes of their V_0 calculations match the scattering length reasonably well. However, we suspect that while the scattering length provides rough guidelines for V_0 at low densities, it is not a reliable metric for judging the accuracy of the V_0 calculation (discussed further in section III C). Moreover, their calculation requires the input of the scattering length and makes more assumptions regarding the potential interaction. Therefore, we believe the differences come from both the representation of the pseudo-potential, which has an effect on both the positron-atom interaction and the form of the ansatz (equation (1)).

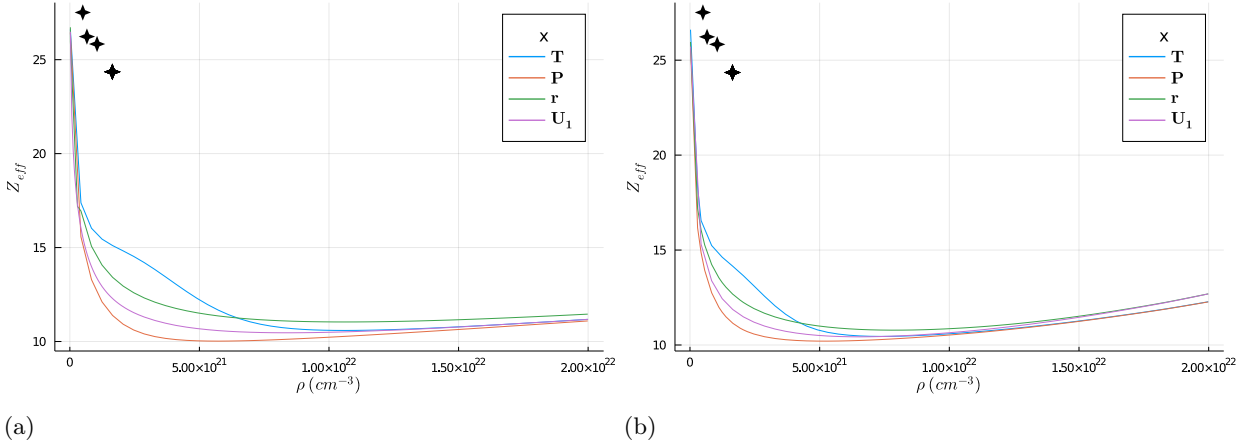


Figure 3: (a) Z_{eff} calculation with $r_{\text{cell}} = r_{WS}$ (b) Z_{eff} calculation with $r_{\text{cell}} = r_{LWS}$. The different lines correspond to the different options for U_2^x , where x is shown in the legend. The black stars in (a) and (b) refer to the experimental data for argon at 295K.⁴⁷

B. Density dependence of Z_{eff} for argon

It is difficult to measure V_0 for positrons in a fluid directly; the only related measurements we are aware of are for positrons in the solid rare gases²⁶. Fortunately, there are many measurements at different densities for the annihilation rate of the rare gases, which is proportional to Z_{eff} . Hence, we have calculated Z_{eff} values for the lowest-energy positron states by using the wavefunction density and its overlap with the atomic orbital densities, and we have compared the results with experimental measurements.

Our calculations for the Z_{eff} values of the positron ground state are shown in figures 3a) and b) for $r_{\text{cell}} = r_{WS}$ and r_{LWS} respectively. The comparison with literature data shows disagreements with our calculation in the density dependence of Z_{eff} . While our calculation matches with literature data at low densities, it seems that the prediction for the ground-state is more sensitive to the density than the experimental measurements of the ensemble average.

The disagreement potentially comes from the fact that this comparison between our calculated Z_{eff} values and the experimental data is not direct. The experimental measurements are an ensemble average of a distribution of positron kinetic energies, while the WS approach only calculates for the lowest energy state. Ideally, the experimental measurements result in a thermal distribution, however, it is often not the case, especially with heavier rare gases⁴⁸. The heavier rare gases have larger Z_{eff} and slower thermalisation rates, therefore they do not allow

the incoming positron beam to thermalise^{49,50}. We expect that the theoretical prediction for the energy shifts of the higher-kinetic-energy states to be smaller in magnitude than V_0 , because they are able to move more freely throughout the fluid. Therefore, the difference between experiment and theory might be exaggerated in this comparison.

As an attempt to investigate this discrepancy between our Z_{eff} and the literature data further, we calculated the averaged effective charge $\langle Z_{\text{eff}} \rangle$. The comparison between $\langle Z_{\text{eff}} \rangle$ and the literature data is shown in Figure 4. As suspected, because the thermal calculation using only the lowest energy orbital is not representative of the thermal average of the system, the kinetic contribution is not enough to fill the gap between our Z_{eff} calculation and the literature data.

C. Density dependence of V_0 and Z_{eff} for all other noble gases

In order to demonstrate the density dependence of V_0 and Z_{eff} for all noble gases, we present the results calculated using the option $U_2^{U_1}$ for U_2 . We chose this method because it can be easily implemented, and it shares similarities with prior pseudo-potential approaches by introducing a clear cut-off point for the potential.

Overall, our calculations exhibit the same qualitative trend as the hard-sphere calculation done by Pleniewicz and co-workers²⁶. Similar with the conclusion we made with argon, their calculations are consistently higher than

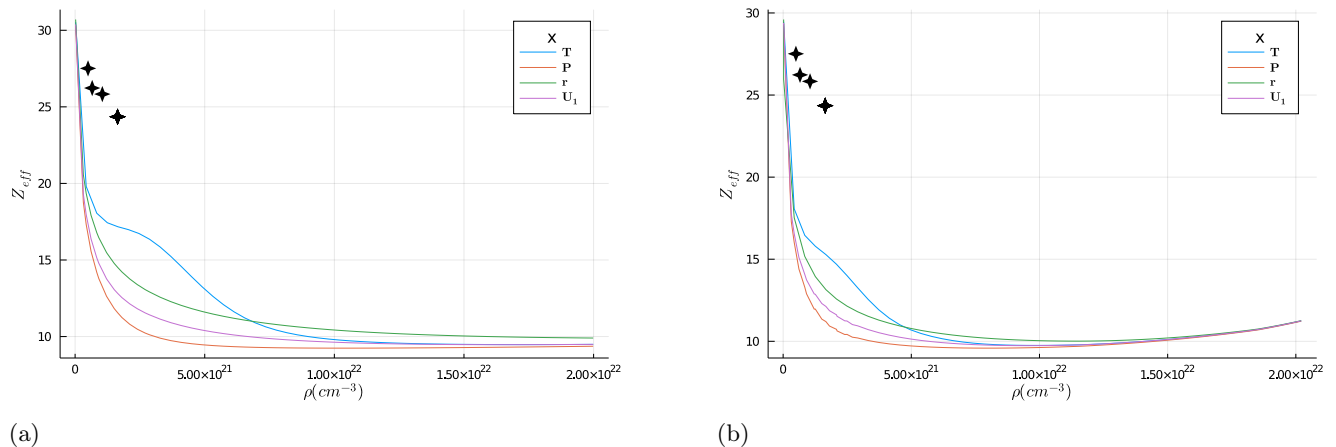


Figure 4: The thermal calculation of density dependence of Z_{eff} for argon at 295K. (a) Z_{eff} for WS radius. (b) Z_{eff} calculation with LWS radius. The different lines correspond to the different options for U_2^x , where x is shown in the legend. The black stars refers to the experimental data for argon at 295K⁴⁷.

our calculations with V_0 . To explore the quantitative differences, we now focus on the fluid effective scattering length, obtained using the slope of V_0 at low densities.

As mentioned before, the scattering length is commonly used as a metric for V_0 in low density regions. In table I we show the scattering lengths calculated using PEEL and the polarized-orbital method of McEachran *et al* in the first and last column^{6–9,52}. The effective scattering lengths in the second and third column were calculated using the slope of V_0 as $\rho \rightarrow 0$. The comparison shows the influence of the background energy V_0 on the scattering lengths.

Overall, the effective scattering lengths are different from the single-atom scattering lengths, and the difference grows with the atomic weights of the elements. We also observed that for light elements, the fluid environment becomes more attractive compared to single scattering, while for heavy elements (xenon), the trend is the opposite; this is interesting. The strong deviation of the fluid effective scattering length implies that it is a poor approximation to use the single-atom scattering length in fluid calculations. We suspect that the contact potential approximation employed by equation (28) does not hold for even dilute regions. In addition, the surrounding average assumption in the Wigner-Seitz theory is unlikely to capture elements with higher polarizability, so further deviation of the effective scattering length can occur.

In terms of the density dependence of V_0 and Z_{eff} , all noble gases show similar behaviours. The sharper drop of Z_{eff} observed in argon is also observed in other noble gases. The disagreement between our calculated results

and literature data is more obvious with heavier elements. Again, we suspect that the Wigner-Seitz theory averages over significant many-body interactions that are due to the large polarizability of the heavier elements.

Similar with our observation in argon, the drastic difference in the V_0 calculation with WS and LWS radius is not reflected in the corresponding Z_{eff} values (See Figure 5). In order to help understand why there is lack of correspondence between the behaviours of V_0 and Z_{eff} , we also considered observing the ratios of these calculated quantities. A strong link between Z_{eff} and V_0 has been identified by Iakubov *et al*⁵. By comparing the form of the two equations for the evaluation of these terms, Iakubov were able to show that a contact potential gives rise to the relation:

$$\frac{Z_{\text{eff}}}{(Z_{\text{eff}})_{\rho \rightarrow 0}} \approx \frac{V_0/\rho}{(V_0/\rho)_{\rho \rightarrow 0}} \quad (29)$$

that is, the ratio of Z_{eff} to its atomic value (shown here as the limit of zero density) is equal to the ratio of the intensive quantity, background energy per density, to its atomic value.

We have calculated the ratios on the left- and right-sides of equation (29), and shown them in figure (6). For the case of WS radius, we find little agreement with equation ((29)) for heavy elements, while it seems to do reasonably well for light elements such as helium and neon. While in the case of LWS radius, the disagreement starts earlier (neon), but the disagreements for heavier elements seem to be lessened compared to the case with WS radius.

We believe this behaviour is the result of one or more

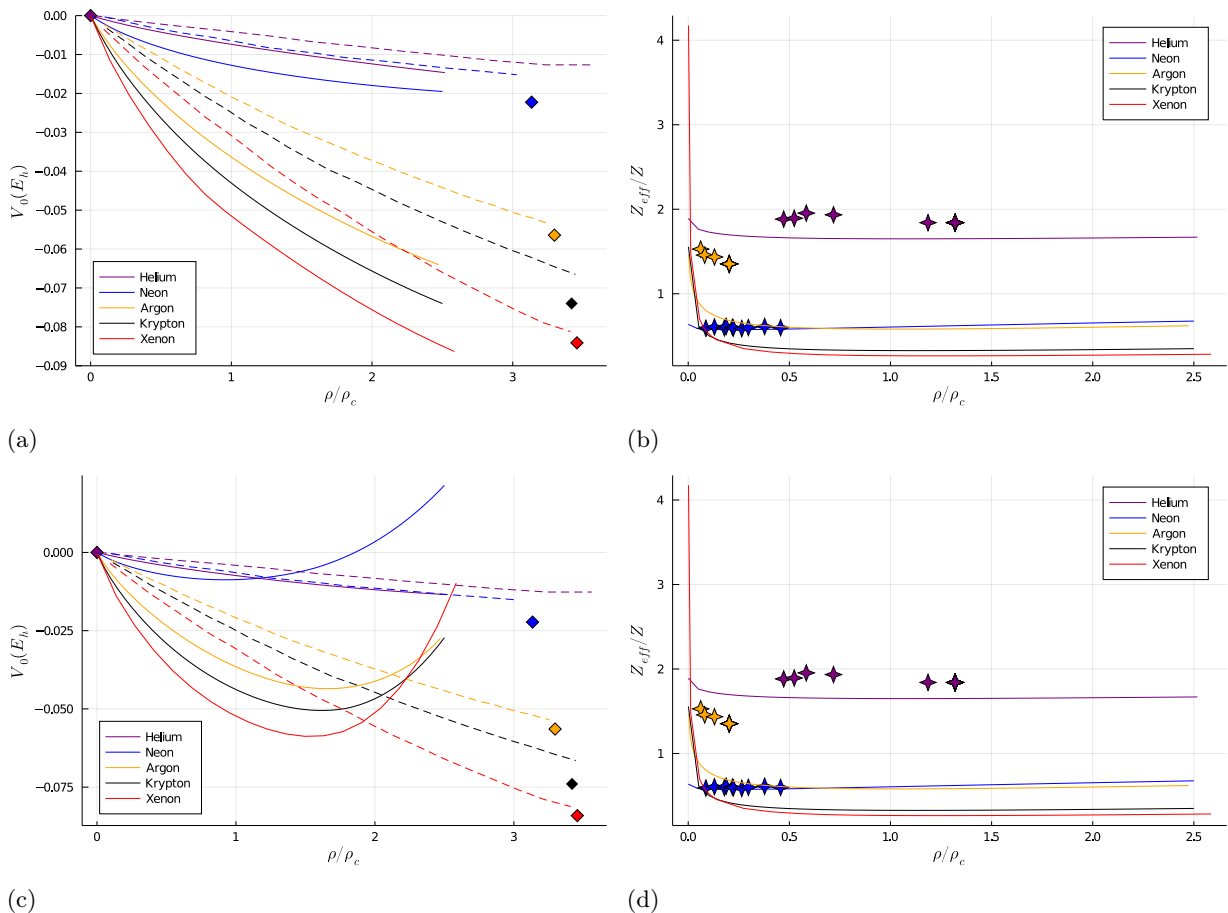


Figure 5: The density dependence of V_0 and Z_{eff} is shown in solid lines for all gases using WS/LWS radius: helium, neon, argon, krypton, and xenon. ρ/ρ_c is the ratio between the density and the critical density, and Z_{eff}/Z is the ratio between the Z_{eff} and Z , the atomic number. (a) V_0 calculation using the option U_2^{U1} using WS radius (b) Z_{eff} calculation using the option U_2^{U1} using WS radius. (c) V_0 calculation using the option U_2^{U1} using LWS radius. (d) Z_{eff} calculation using the option U_2^{U1} using LWS radius. The temperatures for helium, neon, argon, krypton, xenon are 77K, 77.3K, 295K, 297K, 300K respectively. The dashed lines in (a) and (c) come from the theoretical studies using a hard-sphere potential²⁶. The diamonds in (a) and (c) refer to the experimental results obtained in crystalline samples at 4 K⁴⁵. The star symbol in (b) (d) represents literature data^{12,47,49-51}.

of three factors. Either the contact potential origins of equation (29) cause it to be invalid for real atomic gases, or our calculations for heavy elements lack of something important, or the method in which we have calculated Z_{eff} is inappropriate; all three factors have been discussed above. It is our aim to resolve this discrepancy in the future by calculating an approximate transition matrix for the motion of the positron in the fluid without recourse to a surrounding average.

IV. CONCLUSION

In this paper we present the results of different options regarding the WS calculation of V_0 of positron in noble gases (He, Ne, Ar, Kr, and Xe). In terms of the calculation itself, several options for the potential and WS radius were discussed. We have also commented on several options in the evaluation of V_0 results.

In contrast to previous theoretical calculations using pseudo-potentials, we have employed *ab initio* potentials

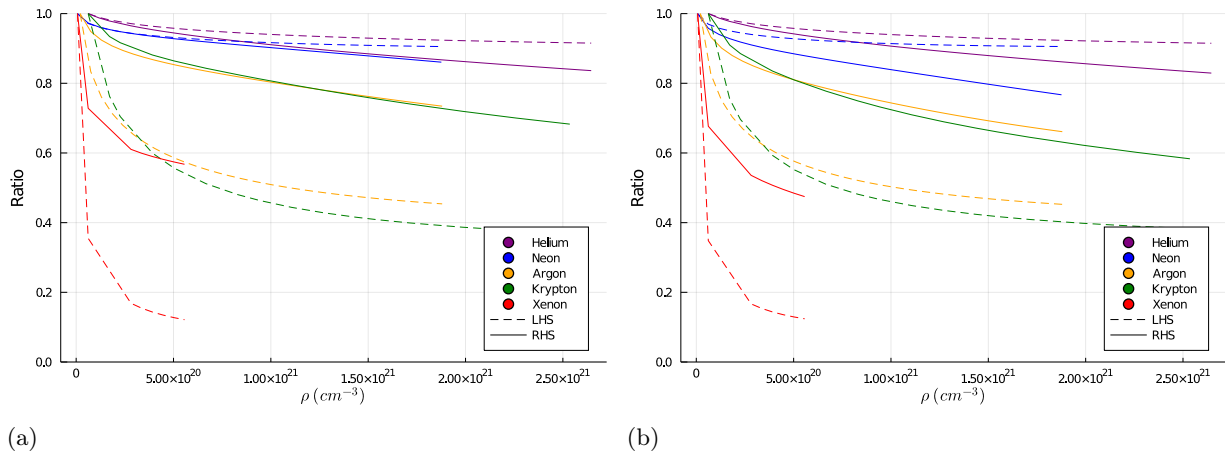


Figure 6: The comparison stated by equation (29) for (a) WS radius and (b) LWS radius. The y-axis shows the ratio of the right hand side and the left hand side of the equation respectively. The different colors correspond to different noble gases, and the dashed and solid lines refer to the LHS and RHS of the equation (29).

| | Atomic | LWS | WS | McEachran |
|---------|--------|--------|--------|-----------|
| Helium | -0.45 | -1.01 | -1.00 | -0.48 |
| Neon | -0.55 | -1.55 | -1.55 | -0.61 |
| Argon | -5.40 | -7.64 | -6.98 | -5.30 |
| Krypton | -11.21 | -11.95 | -10.39 | -10.37 |
| Xenon | -67.80 | -14.48 | -13.42 | -45.32 |

Table I: The first three columns were produced by PEEL. The first column is our single scattering calculation for positron-atom collision. The second and third column are our effective scattering lengths calculated in fluids for the purpose of comparing with single scattering. The last column is the single scattering calculations done by McEachran *et al*^{6-9,52}. The differences between the first and final column are due to some revised parameters in the potential calculation.

to describe the interaction between the positron and the liquid atoms, and we have shown the effects of different options for cut-offs applied for the positron-environment interaction. Among all four options proposed, the U_2^T exhibits the most unusual trend. We believe that the strangeness of the cut-off U_2^T is due to the over-estimation of the repulsive interaction at low densities. All other three options produce similar trends but differ in the relative positions. While U_2^P consistently serves as a lower bound, the relative positions of other three options change with increasing densities. We chose $U_2^{U_1}$ as the potential option for the calculations for all noble gases, but it does

not mean we believe that is the best option.

In order to evaluate our V_0 results, we have made several attempts. There is no direct experimental data for V_0 values for positron in fluids; therefore, we calculated Z_{eff} . This indirect comparison carries flaws as the experimentally measured Z_{eff} comes from positrons with a thermal distribution, while our approach only calculates the lowest energy state of the positron. As a result, our Z_{eff} results match with literature data reasonably well for light noble gases (He and Ne), while being consistently lower for heavier elements at higher densities. We implemented a preliminary calculation using a thermal distribution of positrons, but the results were not ideal. We believe the thermal calculation with only the lowest energy state is not enough, and more calculations are needed in order to properly use Z_{eff} as a metric for evaluating V_0 calculations.

We have also tried to compare the V_0 calculations at low densities to the results of contact potential calculations. We have compared the effective scattering lengths calculated from slopes in V_0 at low densities with the scattering lengths in different gases. The difference between the two is undeniable, and it grows larger for heavier elements. The large differences between the fluid effective and single scattering lengths suggest that the contact potential approximation using the single scattering length is a poor choice for fluid calculations. The limitations of using an ensemble average for part of the potential in the Wigner-Seitz theory, we believe, further contributes to this deviation for heavier elements. We have also compared our results to the equation (29), and it has shown

reasonable agreement for light elements but not for heavy elements. Again, we believe the disagreement is the result of both the contact potential approximation and the surrounding average assumption of the Wigner-Seitz theory.

We have also shown the V_0 results using WS and LWS radius. Previously V_0 calculations using LWS radius for electrons were shown to be promising¹⁶; while turning points in V_0 were observed using LWS radius, it is not conclusive that LWS radius is more accurate than WS radius because the corresponding Z_{eff} calculations for WS and LWS radius show little difference.

In conclusion, we believe that we have used a more *ab initio* potential to obtain V_0 for positrons in fluids, and we have examined several options for the potential calculation and the evaluation methods for V_0 results. For most of the potential options we provided, we have obtained reasonable agreements with indirect literature data for light elements (He and Ne), but unsatisfactory agreements for heavier elements. We believe that the Wigner-Seitz theory has limitations for calculating heavier elements with higher polarisibilities.

In future work, we will consider employing a diagrammatic expansions³⁷ of the many-body interaction to describe propagating states³⁸ directly and represent the observable quantities, such as energy, dispersion and annihilation rate. We believe this will ideally lead us to determining the most appropriate option for the ansatz in the Wigner-Seitz theory for the potential ensemble average. In terms of Z_{eff} calculations, we will consider the full nonequilibrium dynamics in transport simulations to more accurately compare with experimental observations²⁷.

DATA AVAILABILITY

The data that support the findings of this study are available from the corresponding author upon reasonable request.

REFERENCES

- ¹Patrick Vanraes and Annemie Bogaerts. Plasma physics of liquids—a focused review. *Applied Physics Reviews*, 5(3):031103, 2018.
- ²T Jones. The application of positron-emission tomography. In *Computed emission tomography*. 1982.
- ³David J Parker and Xianfeng Fan. Positron emission particle tracking—application and labelling techniques. *Particulology*, 6(1):16–23, 2008.
- ⁴Daniel G Cocks and Ron D White. Excitation processes as a pathway for electron solvation in non-polar liquids. In *2019 IEEE 20th International Conference on Dielectric Liquids (ICDL)*, pages 1–4. IEEE, 2019.
- ⁵I. T. Iakubov and A. G. Khrapak. Self-trapped states of positrons and positronium in dense gases in liquids. *Reports on Progress in Physics*, 45(7):697–751, 1982. ISSN 00344885. doi:10.1088/0034-4885/45/7/001.
- ⁶RP McEachran, AG Ryman, and AD Stauffer. Positron scattering from argon. *Journal of Physics B: Atomic and Molecular Physics*, 12(6):1031, 1979.
- ⁷RP McEachran, AD Stauffer, and LEM Campbell. Positron scattering from krypton and xenon. *Journal of Physics B: Atomic and Molecular Physics*, 13(6):1281, 1980.
- ⁸RP McEachran, AG Ryman, AD Stauffer, and DL Morgan. Positron scattering from noble gases. *Journal of Physics B: Atomic and Molecular Physics*, 10(4):663, 1977.
- ⁹RP McEachran and AD Stauffer. Elastic scattering of electrons from neon and argon. *Journal of Physics B: Atomic and Molecular Physics*, 16(21):4023, 1983.
- ¹⁰Michael Rosenblit and Joshua Jortner. Dynamics of excess electron localization in liquid helium and neon. *Journal of Physical Chemistry A*, 101(4):751–757, 1997. ISSN 10895639. doi: 10.1021/jp962625i.
- ¹¹B. Plenkiewicz, J. P. Jay-Gerin, P. Plenkiewicz, and G. B. Bachelet. Conduction band energy of excess electrons in liquid argon. *Epl*, 1(9):455–460, 1986. ISSN 12864854. doi:10.1209/0295-5075/1/9/006.
- ¹²R. M. Nieminen. Nonlinear density dependence of the positron decay rate in helium. *Physical Review A*, 21(4):1347–1349, 1980. ISSN 10502947. doi:10.1103/PhysRevA.21.1347.
- ¹³P. Van Reeth and J. W. Humberston. Energy dependence of the annihilation rate in positron-atom scattering. *Journal of Physics B: Atomic, Molecular and Optical Physics*, 31(5), 1998. ISSN 09534075. doi:10.1088/0953-4075/31/5/004.
- ¹⁴DG Green, JA Ludlow, and GF Gribakin. Positron scattering and annihilation on noble-gas atoms. *Physical Review A*, 90(3): 032712, 2014.
- ¹⁵A. F. Borghesani. Resonant electron attachment to oxygen impurities in dense Neon gas. *Proceedings of the 2014 IEEE 18th International Conference on Dielectric Liquids, ICDL 2014*, 2014. doi:10.1109/ICDL.2014.6893070.
- ¹⁶C. M. Evans and G. L. Findley. Energy of the conduction band in near critical point fluids. *Physics Research International*, 2010, 2010. ISSN 1687689X. doi:10.1155/2010/749293.
- ¹⁷R Reininger, U Asaf, IT Steinberger, and S Basak. Relationship between the energy v_0 of the quasi-free-electron and its mobility in fluid argon, krypton, and xenon. *Physical Review B*, 28(8): 4426, 1983.
- ¹⁸U Asaf, R Reininger, and IT Steinberger. The energy v_0 of the quasi-free electron in gaseous, liquid and solid methane. *Chemical physics letters*, 100(4):363–366, 1983.
- ¹⁹Xianbo Shi, Luxi Li, Gina M. Moriarty, C. M. Evans, and G. L. Findley. Energy of the quasi-free electron in low density Ar and Kr: Extension of the local Wigner-Seitz model. *Chemical Physics Letters*, 454(1-3):12–16, 2008. ISSN 00092614. doi: 10.1016/j.cplett.2008.01.060.
- ²⁰C. M. Evans, Kamil Krynski, Zachary Streeter, and G. L. Findley. Energy of the quasi-free electron in H₂, D₂, and O₂: Probing intermolecular potentials within the local Wigner-Seitz model. *Journal of Chemical Physics*, 143(22), 2015. ISSN 00219606. doi: 10.1063/1.4936627.
- ²¹Yevgeniy Lushtak, Samantha B. Dannenberg, C. M. Evans, and G. L. Findley. Quasi-free electron energy in near critical point helium. *Chemical Physics Letters*, 538:46–49, 2012. ISSN 00092614.

- doi:10.1016/j.cplett.2012.04.026. URL <http://dx.doi.org/10.1016/j.cplett.2012.04.026>.
- ²²Xianbo Shi, Luxi Li, C. M. Evans, and G. L. Findley. Energy of the quasi-free electron in argon, krypton and xenon. *Nuclear Instruments and Methods in Physics Research, Section A: Accelerators, Spectrometers, Detectors and Associated Equipment*, 582(1):270–273, 2007. ISSN 01689002. doi: 10.1016/j.nima.2007.08.129.
- ²³C. M. Evans and G. L. Findley. Energy of the quasifree electron in argon and krypton. *Physical Review A - Atomic, Molecular, and Optical Physics*, 72(2):22–24, 2005. ISSN 10502947. doi: 10.1103/PhysRevA.72.022717.
- ²⁴C. M. Evans, Yevgeniy Lushtak, and G. L. Findley. Energy of the quasi-free electron in dense neon. *Chemical Physics Letters*, 501(4-6):202–205, 2011. ISSN 00092614. doi: 10.1016/j.cplett.2010.11.019. URL <http://dx.doi.org/10.1016/j.cplett.2010.11.019>.
- ²⁵Xianbo Shi, Luxi Li, G. L. Findley, and C. M. Evans. Energy of the excess electron in methane and ethane near the critical point. *Chemical Physics Letters*, 481(4-6):183–189, 2009. ISSN 00092614. doi:10.1016/j.cplett.2009.09.100. URL <http://dx.doi.org/10.1016/j.cplett.2009.09.100>.
- ²⁶B Plenkiewicz, Y Frongillo, J-M Lopez-Castillo, and J-P Jay-Gerin. A simple but accurate “core-tail” pseudopotential approach to the calculation of the conduction-band energy v_0 of quasifree excess electrons and positrons in nonpolar fluids. *The Journal of chemical physics*, 104(22):9053–9057, 1996.
- ²⁷DG Cocks, RP McEachran, GJ Boyle, E Cheng, and RD White. Positron scattering and transport in liquid helium. *Journal of Physics B: Atomic, Molecular and Optical Physics*, 53(22): 225201, 2020.
- ²⁸D Chandler. Excess Electrons in Liquids: Geometrical Perspectives. *Annual Review of Physical Chemistry*, 45(1):557–591, 1994. ISSN 0066426X. doi:10.1146/annurev.physchem.45.1.557.
- ²⁹B. Space, D. F. Coker, Z. H. Liu, B. J. Berne, and G. Martyna. Density dependence of excess electronic ground-state energies in simple atomic fluids. *The Journal of Chemical Physics*, 97(3): 2002–2021, 1992. ISSN 00219606. doi:10.1063/1.463138.
- ³⁰David Cubero, Nicholas Quirke, and David F Coker. Electronic transport in disordered n-alkanes: From fluid methane to amorphous polyethylene. *The Journal of chemical physics*, 119(5): 2669–2679, 2003.
- ³¹B. E. Springett, J. Jortner, and M. H. Cohen. Stability criterion for the localization of an excess electron in a nonpolar fluid. *The Journal of Chemical Physics*, 48(6):2720, 1968. ISSN 00219606. doi:10.1063/1.1669506.
- ³²Richard A Holroyd and Werner F Schmidt. Transport of electrons in nonpolar fluids. *Annual Review of Physical Chemistry*, 40(1): 439–468, 1989.
- ³³B Boltjes, C De Graaf, and SW De Leeuw. Computation of the energy v_0 of an excess electron in dense helium and argon. *The Journal of chemical physics*, 98(1):592–601, 1993.
- ³⁴B Plenkiewicz, P Plenkiewicz, J-P Jay-Gerin, and Ashok K Jain. Density dependence of the ground-state energy of excess electrons in liquid methane. *The Journal of chemical physics*, 90(9):4907–4908, 1989.
- ³⁵B Plenkiewicz, P Plenkiewicz, and J-P Jay-Gerin. Pseudopotential calculations for elastic scattering of slow electrons (0–20 eV) from noble gases. i. argon. *Physical Review A*, 38(9):4460, 1988.
- ³⁶R. Reininger, U. Asaf, I. T. Steinberger, and S. Basak. Relationship between the energy V_0 of the quasi-free-electron and its mobility in fluid argon, krypton, and xenon. *Physical Review B*, 28(8):4426–4432, 1983. ISSN 01631829. doi: 10.1103/PhysRevB.28.4426.
- ³⁷A Ya Polischuk. Theory of electron mobility in moderately dense polar gases. *Journal of Physics B: Atomic and Molecular Physics*, 18(4):829–841, feb 1985. ISSN 0022-3700. doi:10.1088/0022-3700/18/4/024. URL <http://stacks.iop.org/0022-3700/18/i=4/a=024?key=crossref.58647f8fd759703edc442ec655faacdb>.
- ³⁸Melvin Lax. Multiple Scattering of Waves. *Reviews of Modern Physics*, 23(4):287–310, oct 1951. ISSN 0034-6861. doi: 10.1103/RevModPhys.23.287. URL <https://link.aps.org/doi/10.1103/RevModPhys.23.287>.
- ³⁹GJ Boyle, Robert P McEachran, DG Cocks, and Ron D White. Electron scattering and transport in liquid argon. *The Journal of chemical physics*, 142(15):154507, 2015.
- ⁴⁰R P McEachran, A G Ryman, A D Stauffer, and D L Morgan. Positron scattering from noble gases. *Journal of Physics B: Atomic and Molecular Physics*, 10(4): 663–677, mar 1977. ISSN 0022-3700. doi:10.1088/0022-3700/10/4/018. URL <http://stacks.iop.org/0022-3700/10/i=4/a=018?key=crossref.01f2c995d7d2462925bd66c6e2123d15>.
- ⁴¹J. Lekner. Motion of electrons in liquid argon. *Physical Review*, 158(1):130–137, 1967. ISSN 0031899X. doi: 10.1103/PhysRev.158.130.
- ⁴²Jean-Pierre Hansen and Ian R McDonald. *Theory of simple liquids*. Elsevier, 1990.
- ⁴³Seung-Kyo Oh. Modified lennard-jones potentials with a reduced temperature-correction parameter for calculating thermodynamic and transport properties: Noble gases and their mixtures (he, ne, ar, kr, and xe). *Journal of thermodynamics*, 2013, 2013.
- ⁴⁴Steve Plimpton. Fast parallel algorithms for short-range molecular dynamics. *Journal of computational physics*, 117(1):1–19, 1995.
- ⁴⁵EM Gullikson, AP Mills Jr, and EG McRae. Observation of intense two-beam positron diffraction and the precise determination of the positron band gap in rare-gas crystals. *Physical Review B*, 37(1):588, 1988.
- ⁴⁶P. Hautojärvi, K. Ryttsölä, P. Tuovinen, A. Vehanen, and P. Jauho. Microscopic Gas-Liquid-Like Phase Transition around the Positron in Helium Gases. *Physical Review Letters*, 38(15):842–844, apr 1977. ISSN 0031-9007. doi: 10.1103/PhysRevLett.38.842. URL <http://link.aps.org/doi/10.1103/PhysRevLett.38.842>.
- ⁴⁷M Tuomisaari, Klaus Ryttsölä, and P Hautojärvi. Localized state of positron in argon. *Physics Letters A*, 112(6-7):279–282, 1985.
- ⁴⁸DG Green. Positron cooling and annihilation in noble gases. *Physical review letters*, 119(20):203403, 2017.
- ⁴⁹M Tuomisaari, K Ryttsola, and P Hautojarvi. Positron annihilation in xenon. *Journal of Physics B: Atomic, Molecular and Optical Physics*, 21(23):3917, 1988.
- ⁵⁰GL Wright, M Charlton, TC Griffith, and GR Heyland. The annihilation of positrons and positronium formation in gaseous kr and xe. *Journal of Physics B: Atomic and Molecular Physics*, 18(21):4327, 1985.
- ⁵¹KF Canter and LO Roellig. Positron annihilation in low-temperature rare gases. ii. argon and neon. *Physical Review A*, 12(2):386, 1975.
- ⁵²RP McEachran and AD Stauffer. Positron scattering from helium. *Journal of Physics B: Atomic, Molecular and Optical Physics*, 52(11):115203, 2019.